Geophys. J. R. astr. Soc. (1978) **55**, 411–434

Stress and temperature in subduction shear zones: Tonga and Mariana

Peter Bird *Department of Earth and Space Sciences, University of California, Los Angeles, USA*

Received 1978 April 13; in original form 1977 December 19

Summary. Because there is secondary sea-floor spreading in the Tonga and Mariana subduction systems, the island arcs are separate plates. Horizontal forces on the two sides of the arc must balance, and the maximum force on the back-arc side can be calculated from a lithostatic ridge model. This, in combination with gravity data, allows calculation of the average shear stress in the top 100 km of the subduction shear zone. Stress in Tonga is 220 ± 100 bar, and in the Mariana it is 165 ± 75 bar. These low stresses are probably made possible by a fluid pore pressure almost equal to the least compressive stress.

Knowledge of stress allows approximate calculation of temperature in the shear zone by integration of a single differential equation. These temperatures are too low to activate most dehydration reactions in the subducted crust. As it approaches the volcanic line, this crust is at 150–350°C in Tonga and 150–300°C in the Mariana. Shear melting of the crust is ruled out, and conductive melting of the slab by contact with the asthenosphere meets with geochemical objections. Magmas in these systems are probably produced by partial melting of asthenosphere, triggered by a sudden release of water from the slab.

1 Introduction

One of the most persistent and troublesome unknowns in the study and modelling of subduction zones is the amount of shear stress between the two interacting plates. This stress is responsible for most of the world's largest earthquakes, whose mechanism is still not well understood. Through shear-strain heating, it contributes a part of the energy that warms the subducted crust and sediments as they travel from the trench to beneath the island arc. Ignorance of stress thus implies ignorance of temperature. This prevents any quantitative understanding of the metamorphic reactions in subduction zones, the amount of water carried down into the mantle, or the origin of island-arc magmas.

Plausible estimates of this stress have spanned two orders of magnitude. On the high side, application of a Coulomb friction law implies shear stresses of order 20 kbar at 90 km depth. Hasebe, Fujii & Uyeda (1970) explained the high heat flow behind arcs with a shear

of about 600 bar at the top of the slab. Turcotte & Schubert (1973) derived a value of 1.4 kbar by requiring friction to cause the melting of island-arc magmas. However, Sleep (1973) found in a finite-difference calculation that 4 kbar of stress is required to cause a positive temperature anomaly above the slab. Sleep (1975) estimated stress in the Aleutian subduction zone to be about 200 bar, in flow models where the interaction of stress, gravity and topography was studied. Yuen *et al.* (1978) solved the time-dependent shearing problem, and obtained stresses between several hundred bars (for a diabase flow law) and a few bars (for limestone). Blackwell & Ziagos (1977) used the heat flow above the mid-American subduction zone to estimate its stress at around 900 bar. A lower limit is provided by the seismic stress drops in shallow sub-trench earthquakes, which, with a few rare exceptions, (Wyss 1970) are less than 100 bar.

To date, the only quantities used to constrain this stress are the available potential body force on the slab and the surface heat flow. However, it is unclear what fraction of the frictional heat reaches the surface, particularly when the heat absorption of dehydration reactions (Anderson, Uyeda & Miyashiro 1976) is considered. This study uses a different approach, by looking at two island arcs where a force balance can be constructed. Since the shear stress between plates is the major unknown in this balance, it can be determined within an uncertainty of 100 bar. This in turn allows the calculation of slab-surface temperatures for steady-state subduction within 100°. The conclusion that shear stress and frictional heating are very small has important implications for the problem of island-arc earthquake and magma genesis.

2 Stress in the upper shear zone

In a subduction system which includes back-arc spreading the geometry of lithosphere and asthenosphere is probably like that illustrated in Fig. 1. The island arc is a long thin plate, in contact with the atmosphere and ocean above, the asthenosphere below and on the back-arc side, and the subducting plate to the fore-arc side. If the island arc portion of the system is isolated (as by the dashed line in Fig. 1) and we consider all the forces acting upon it, they must sum to zero because the arc is not accelerating. It is particularly useful (to avoid calculating the force of gravity upon unknown masses) to concentrate on horizontal forces in the direction perpendicular to the strike of the trench. Except where the arc forms the upper boundary of the subduction shear zone, it is in contact with materials of no long-term strength (air, water, asthenosphere). If deviatoric stresses in these fluids are small, then a

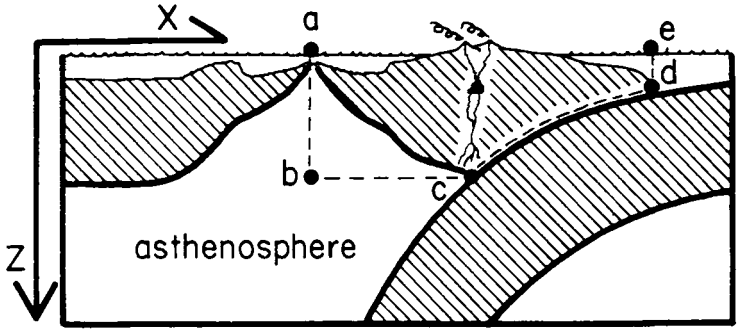

Figure 1. Schematic cross-section of an island arc with a subduction zone on the right and back-arc seafloor spreading on the left. The island arc is a separate plate, and horizontal forces exerted on the area outlined with the dashed line must balance.

hydrostatic or lithostatic approximation will yield the forces exerted on these boundaries, which must be balanced by forces arising from stress in the shear zone. (Transmission of deviatoric stress between the slab and arc is assumed to terminate at the point at which magma is generated. Thus the values of shear stress to be obtained will be averages for that part of the subduction shear zone above 100 km depth.)

To translate this physical principle into a formula for subduction zone stresses, four simplifying assumptions were employed:

(1) The asthenosphere is a perfect fluid of constant density ρ_a.
(2) At the centre of the secondary-spreading ridge, this asthenosphere rises to a level determined by isostasy, separating the adjacent plates.
(3) In the shear zone, principal stress axes are at an angle of 45° to its surface; the interplate fault is a surface of maximum shear stress.
(4) In the shear zone, the vertical stress σ_{zz} is equal to the weight of the overlying rock and water.

The calculation of the shear stress where the plates interact proceeds in the following way. Because of the first assumption, there can be no shear tractions on the base of the island arc plate. Therefore the force exerted by lithostatic and hydrostatic pressure on the back-arc side must be balanced by a combination of normal and shear forces on the trench side. The second assumption makes the calculation of back-arc pressure elementary. However, in the shear zone there may be a complex state of stress characterized by three unknowns: the pressure, the deviatoric stress and the dip of the greatest compression direction. Two of these unknowns must be eliminated before the force balance constraint can be used to solve for the third. In this paper, assumption (3) is used to estimate deviatoric stress orientation, and assumption (4) to eliminate one more degree of freedom. The result is that the integral of the shear stress opposing subduction (and hence its average value) is uniquely determined.

The details of the mathematic derivation are contained in Appendix A, which makes use of the assumptions above in reducing the complex reality to a straightforward formula. Later, in Section 2, the amount of error introduced by these simplifications is shown to be only a fraction of the calculated result.

The difficult step in the application of this method is the calculation of σ_{zz} in the subduction zone. Even using (4) does not make the estimation of overburden from topography straightforward, because the island arc plate is a complex assemblage of sediments, mantle, intrusive and extrusive rocks whose densities and geometries are poorly known. In this work, the overburden weights were constrained by the difference between observed gravity anomalies and a simple model for the attraction of the slab. This process requires only one density to be assumed, the density of the asthenosphere (ρ_a). As long as the same density is used in all equations, any errors introduced by an incorrect value will tend to cancel.

Consider a hypothetical (non-isostatic) geometry as shown in Fig. 2. A plate of denser lithosphere is partly overlying and partly subducted into a constant-density asthenosphere. The gravity anomaly of this structure can be calculated if the excess density of the lithosphere and its subsurface geometry are specified. As on the real Earth, the reference strength in the definition of the gravity anomaly is the value of the attraction over the flat-lying lithosphere.

The excess mass per unit area of lithosphere with respect to asthenosphere is easily obtained from the difference in depth between spreading ridges (h) and the deep ocean outside the outer rise (f). If these two provinces are in isostatic equilibrium (Sclater, Anderson & Bell 1971), then this mass excess is just $(f - h)(\rho_a \quad \rho_w)$. The model gravity

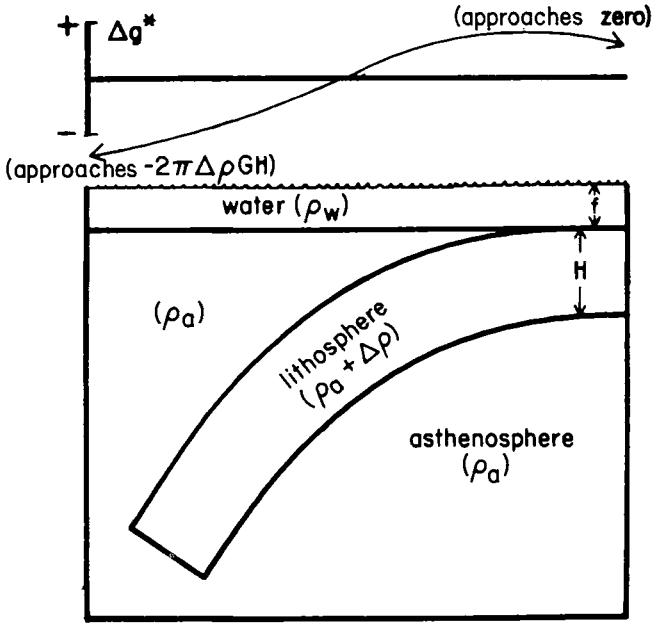

Figure 2. Sketch of a hypothetical density distribution used in calculating a model gravity curve for the effect of the downgoing slab (above). In practice, the shape of the slab in each zone is determined by hypocentre locations.

anomaly $\Delta g^*(x)$ shown in Fig. 2 results from the downward rotation of the lithosphere, and is calculated numerically using a digitized slab profile (down to 700 km depth) from hypocentre determinations.

The reason for introducing this model is that in the model both the gravity anomaly and the weight of the overburden on the slab are known. This gives a first approximation to the vertical stress in the subduction zone, σ_{zz}. This estimate is corrected by an amount proportional to the difference between the actual and model gravity profiles above each point. If the actual gravity is greater than in the model, then some excess density (relative to the model) must be present above the shear zone, where it would contribute to the vertical stress σ_{zz} which we need to determine.

By this method the number of parameters which must be estimated is greatly reduced. For example, any other reference density structure could be substituted above the slab in Fig. 2 without affecting the result. In this paper the shear stress estimates are determined by a balance between unequivocal observables; the ocean's depth and gravity. The important terms in this balance are the depth of the back-arc ridge and the depth of the trench. Because the trench is deeper, horizontal forces exerted by the slab must be greater than lithostatic to compensate. This basically determines the amount of shear stress between the plates, with the gravity term as a small correction.

2.1 STRESS BELOW TONGA

The existence of secondary spreading along the Lau–Havre Trough behind the Tonga island arc has been demonstrated by Karig (1970, 1971a) and by Weissel (1977). Since the Trough is nearly parallel to the Trench, the two-dimensional geometry of Fig. 1 is a good approximation. Thus the average shear stress in the Tongan subduction shear zone to a depth of

Table 1. Stress calculation parameters and estimated errors.

Parameter	Symbol	Tonga Value (V)	Tonga Probable error (δV)	Tonga $\delta V \frac{\partial \bar{\tau}}{\partial V}$	Mariana Value (V)	Mariana Probable error (δV)	Mariana $\delta V \frac{\partial \bar{\tau}}{\partial V}$
Earth gravity at surface	g	978.6 cm s^{-2}	—	—	978.4 cm s^{-2}	—	—
Density of sea-water	ρ_w	1.027 g cm^{-3}	—	—	1.027 g cm^{-3}	—	—
Depth of back-arc ridge	h	2250 m	200 m	15 bar	3450 m	110 m	8 bar
Depth to bottom of shear zone	b	100 km	—	—	110 km	—	—
Asthenosphere density	ρ_a	3.125 g cm^{-3}	0.10 g cm^{-3}	10 bar	3.125 g cm^{-3}	0.10 g cm^{-3}	8 bar
Depth of trench bottom	d	10 000 m	300 m	23 bar	8500 m	280 m	20 bar
Depth of Pacific plate prior to subduction	f	5700 m	300 m	23 bar	6200 m	150 m	11 bar
Measured gravity anomaly	Δg	Fig. 3	7 mGal	7 bar	Fig. 5	3 mGal	3 bar
Assumed regional gravity anomaly	Δg_0	0 mGal	10 mGal	8 bar	−15 mGal	15 mGal	12 bar
Gravity anomaly of slab	Δg^*	Fig. 3	12 mGal	11 bar	Fig. 5	13 mGal	10 bar
Average shear stress in shear zone between depths d and b	$\bar{\tau}$ =	220 bar			$\bar{\tau}$ =	165 bar	
Probable error		40 bar				30 bar	
90 per cent confidence limits		±100 bar				±75 bar	

100 km can be calculated from equation (A12) of Appendix A. Using the parameter values contained in Table 1, this stress is 220 bar. This is several times lower than most previous estimates of stress in any subduction zone, excepting Sleep's (1975) treatment of the Aleutians. It should be understood that this is the time and space averaged shear stress, and does not preclude temporarily or locally higher values. This kind of averaged estimate is very valuable because it implies reliable estimates of related quantities, such as the resistance to subduction exerted by the island arc (4.8×10^{15} dyne/cm) or the maximum possible frictional work available for heating the slab (4.8×10^{15} erg cm^{-2}).

The parameters on which this estimate is based include the depth of trench and back-arc ridge the shape of the subducted slab, its excess density, and the gravity anomaly of the total structure. This gravity profile was obtained on 1967 December 9–10 during *Eltanin* Leg 31, reported by Hayes *et al.* (1972). The depths of the Tonga Trench and Lau–Havre Trough were taken from the same source for consistency. In Fig. 3 a typical bathymetric profile from Fisher & Engel (1969) is shown, but this is not used in the calculation. The shape of the subduction zone (Fig. 3) was drawn primarily from the hypocentre locations of Isacks & Barazangi (1977), with further constraints of a 6° dip entering the trench (Karig, Caldwell & Parmentier 1976) and a limit of 60 km distance from seismic station NIU for the closest earthquake (Isacks, Oliver & Sykes 1968). The assumption that earthquakes west of Tonga take place in the upper half of the slab interior was also useful.

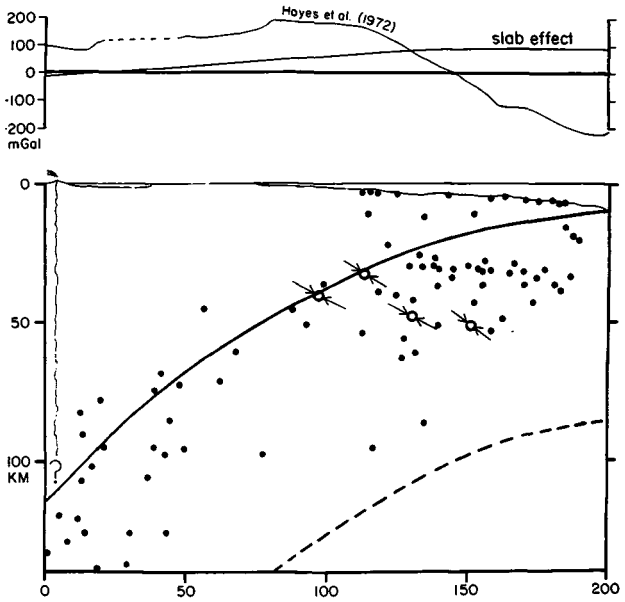

Figure 3. Cross-section of the Tonga island arc and subduction zone (below). Dots indicate hypocentres and arrows give the maximum compression direction from fault-plane solutions. At top, actual free-air gravity data are plotted along with a model curve for the effect of the slab.

Associated with each parameter value in Table 1 is an estimate of its probable error, and also the amount of change in the average stress calculated to result from such an error. If the errors in these parameters are uncorrelated, the probable error of the computed shear stress is 40 bar. Making the usual (unrealistic) assumption of normally distributed errors, the formal 90 per cent confidence limits on this result are ± 100 bar (± 45 per cent). The good precision of this method is a result of its foundation on measurements of depth and gravity, rather than heat flow or seismic radiation.

Of course, the accuracy of this result rests on the validity of the four assumptions of Section 2. The assumption of lithostatic pressure below the Lau–Havre Trough is supported by the lack of a central valley in that spreading centre; Lachenbruch (1976) has shown that such valleys result from viscous resistance to spreading. The assumption of no shear traction on the base of the island arc might seem weak when the probability of induced asthenosphere convection is considered, but Toksöz & Bird (1977) have calculated finite-element models of this flow using a realistic olivine flow law, and found that the net traction is only 10^{14} dyne/cm. The inclusion of such a force in the horizontal force balance would reduce the shear-zone stress by only 4 bar.

One last source of error to consider is assumption (3), that principal stress axes are at 45° to the shear zone. Four fault-plane solutions of Isacks, Sykes & Oliver (1969) are shown in Fig. 3, and for the inferred direction of maximum compression this is not strictly true. In general, if the dip of the actual fault plane is δ at a place where the dip of the shear zone is θ, the estimation of the shear stress on the shear zone will be incorrect by the factor

$$\frac{\tau_{\text{calc}}}{\tau_{\text{act}}} = \frac{2\sin(2\theta)\sin(\delta) + \cos(2\theta)\cos(\delta)}{2\sin(2\delta)\sin(\delta) + \cos(2\delta)\cos(\delta)}.$$

Values of this function for different dips are plotted in Fig. 4, where the four available data are also indicated. If these four events are representative, then the calculated $\bar{\tau}$ should be increased by about 7 per cent to obtain the actual value.

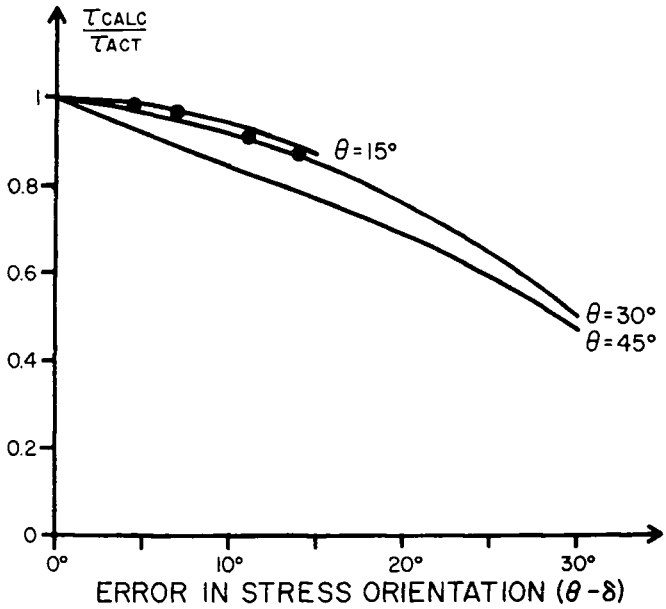

Figure 4. Graph of the function $[2\sin(2\theta)\sin(\delta)+\cos(2\theta)\cos(\delta)]/[2\sin(2\delta)\sin(\delta)+\cos(2\delta)\cos(\delta)]$ as a function of θ and the difference $(\theta-\delta)$. This is the factor by which stress may be miscalculated if the stress orientation (δ) differs from the assumed angle (θ). The four dots represent fault-plane solutions from Fig. 3.

The final assumption, that vertical stress in the shear zone equals overburden weight, need not be true locally. However, it must be true for the whole shear zone in an integral sense, so the effects of departures on the integrated or average value of shear stress will be second-order effects.

2.2 STRESS BELOW THE MARIANAS

Evidence for sea-floor spreading in the Mariana Trough behind the Mariana volcanic arc is given by Karig (1971b) and Anderson (1975). Balancing the forces on the island-arc plate and using the parameter values in Table 1, the average shear stress in the Mariana shear zone to 110 km depth is 165 bar, with a 90 per cent confidence limit of ± 75 bar. Unlike the Tonga result, which was based on data from a single profile, this Mariana stress value is obtained from the averages of many depth and gravity values between 13 and 21° north latitude. It should be interpreted as the average stress throughout this segment of the plate boundary.

The shape of the subduction zone assumed is shown in Fig. 5. It is based on hypocentres located by Katsumata & Sykes (1969), and the bathymetry shown is from Karig (1971b). The depths of trench and trough were obtained from the means of 10 bathymetric profiles from the latter paper. The gravity data available (Watts 1976) between 13 and 21° N were assembled onto a composite section according to distance from the trench axis measured along the direction of relative plate motion. As shown in Fig. 5, these values scatter around their running mean with a standard deviation of 34 mGal, but since there are 137 data the probable error of the mean of the gravity profile is only 3 mGal.

The remarks made in Section 2.1 about the lack of a central valley, effect of induced convection and orientation of principal stresses also apply to the Mariana stress result.

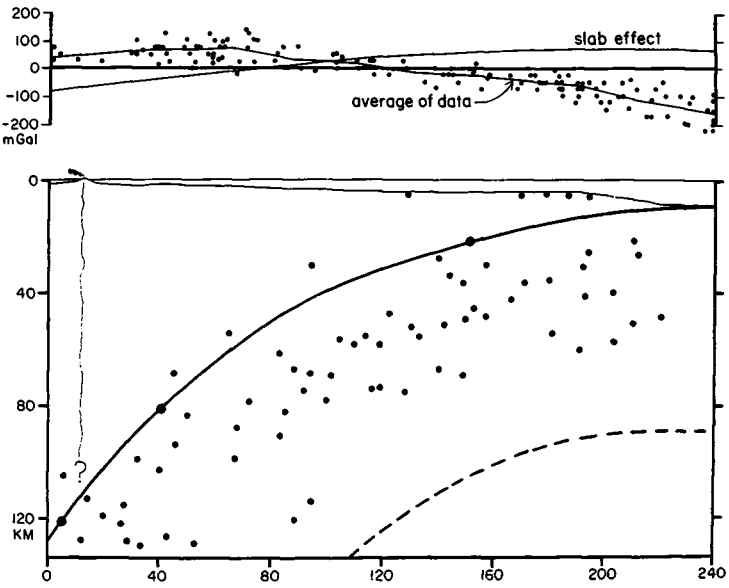

Figure 5. Cross-section of the Mariana island arc and subduction zone. Dots are the locations of hypocentres. Above, gravity data points were used to calculate an average curve, which is compared to the model curve for the slab effect alone.

Unfortunately, the arc is nearly aseismic, so there are no fault-plane solutions with which to test assumption (3). The only indication of a possible problem with the assumptions made is that the Mariana Trough is considerably deeper than the world-wide average for spreading ridges (2750 m according to Le Pichon, Franchetau and Bonnin 1976). Possibly the depth anomalies of this trough (+700 m) and of the Lau–Havre Trough (−500 m) are due to local perturbations of asthenosphere pressure dynamically maintained by the nearby descending slabs. In this case the correct stress result is obtained by employing the actual depths without regard for their causes. Difficulties only arise if the depth anomalies are due to non-hydrostatic stresses below the spreading ridges or to asthenosphere of anomalous density. A possible explanation in the case of the Mariana Trough is that the recent rupture of the lithosphere here has been diffuse rather than sharp, and that a thin cap of old faulted lithosphere overlies the ascending magma. On one hand, this would suggest that the force applied to the island arc will be underestimated, since densities below the ridge may be higher than ρ_a. On the other hand, the shallow horizontal tension in such a non-fluid cap would reduce the total force. Because of the partial cancellation of these two hypothetical effects on the computed shear stress, any error introduced is probably minor.

3 Mechanism of earthquakes and creep

This section, and those following, consider the various implications of the surprisingly low shear stresses in these two subduction zones. Their conclusions are far more qualitative and speculative than those preceding, so it should be emphasized that the stress values already obtained are completely independent of the mechanisms of shear zone deformation, metamorphism and magma genesis which we will consider next. Yet the constraint of a known average stress enables us definitely to reject some of the hypotheses that have been advanced in these areas.

The low average stress in both subduction zones rules out any possibility of simple Coulomb friction (with hydrostatic pore pressure) as the dominant mechanism of shear zone deformation. The remaining possibilities are intragranular creep of a weak mineral (probably calcite), or a nearly lithostatic pore pressure sufficient to reduce the effective and frictional stresses by two orders of magnitude. The first hypothesis fails to explain the high seismicity of the Tonga Trench. The second allows for either seismic or aseismic slip. It can also be shown that the sediment permeabilities it requires are reasonable and that a natural mechanism exists for the regulation of such pore pressures.

As the next section will show, the shear zone temperatures consistent with these low stresses are probably 300°C or less. At such temperatures, only three minerals yet studied show significant amounts of dislocation creep: halite, 'wet' quartz and calcite. Halite has the lowest strength (Heard 1972) but is unlikely among the bathyal sediments of the Pacific sea-floor. 'Wet' quartz has so far only been artifically grown, and not observed in nature. But calcite is almost certainly present in the lower part of the sedimentary column that approaches the Tonga and Mariana trenches (Heezen *et al.* 1973). Significant dislocation creep could occur in calcite under the inferred shear zone conditions (Schmid 1976); and if all of the relative plate motion was accommodated by such creep the predicted stress (Yuen *et al.* 1978) would fall within the calculated range.

The difficulty with this mechanism is that it is inconsistent with shallow thrusting earthquakes in the shear zone below Tonga. Seismic moment rates for the period 1904–52 computed by McGarr (1977) can be combined with plate relative velocities to obtain the width of the seismic zone in the downdip direction. Such a computation for Tonga gives a width of 195 km at a plate velocity (Morgan 1972) of 8.6 cm/yr, or 145 km if we increase the velocity by 3 cm/yr to allow for back-arc spreading. This is 65–90 per cent of the width of the zone modelled, so Tonga is characterized as shearing mainly in seismic jerks. On the other hand, the very small moment sum for the Mariana limits that seismic zone width to a maximum of 35 km, so it is primarily a creeping shear zone.

Since both mechanisms occur at similar stresses and under comparable geologic conditions, it appears that they are not fundamentally different. An analogy with the stick-slip/stable-sliding transition observed during laboratory low-temperature deformation of rocks is suggested. However, since these shear stresses are two orders of magnitude less than those predicted by the Coulomb friction laws that govern that behaviour, there is a serious problem. The mechanism can only be the same if there is a fluid pore pressure in the shear zone almost equal to the least compressive stress.

Such pore pressure could be created by compaction of porous sea-floor sediments after they are dragged into the trench. However, low permeabilities in the shear zones would be required to confine it. The velocity of upward diffusion of pore water would need to be slow compared with plate velocities, while the driving pressure gradient would be the same as the lithostatic pressure gradient. Thus

$$10 \text{ cm/yr} > V = K \rho g \sin(\theta)$$

and the hydraulic permeability K would need to be less than about 10^{-10} cm^4 dyne s^{-1} (or 0.1 mdarcy in conventional units). This is not an implausibly low figure, and so the entrapment of pore water is considered to be a reasonable explanation for the low stresses calculated.

If it seems implausible that the pore pressure should remain so close to the confining pressure without actually attaining it, consider that the permeability is probably a strong function of the difference between total and pore pressure. This is because large populations of cracks are elastically opening and closing in the range where these pressures differ by

0 250 bar (Kuster & Toksöz 1974). This makes possible a self-regulating pore pressure, and the difference between a seismic and an aseismic shear zone is just that the oscillations of pressure are larger in the former.

4 Calculation of steady-state temperatures

The knowledge of approximate shear stresses in these zones makes possible the calculation of temperatures, because friction is a major source of heat. These calculations will assume a steady-state distribution of temperature and flux, since the Tonga islands are at least pre-Upper Eocene in age (Ewart & Bryan 1973) and the Marianas are probably older than the Parece Vela Basin (Karig 1971b), possibly even mid-Eocene (Karig 1975).

Because so little is known about the mechanics of shear zones, it seems premature to concentrate on their internal structure. Of more interest is the variation of temperature in the material along the down-dip direction. For this reason, the computation assumes a thin (1 km?) layer of uniform material, shearing at a uniform strain-rate, and ignores the variation of temperature through its thickness. These are reasonable approximations if the mechanism of deformation is frictional sliding with self-regulating pore pressure, as suggested above. Such a mechanism could only occur in a thin sedimentary or upper crustal layer, and would not be sensitive to variations of temperature or pressure.

This leaves only a single unknown variable, the shear-zone temperature (T), varying as a function of distance down-dip (s). Since the shear zone material is flowing down at an average velocity equal to half the subducting plate velocity (V), its past history at shallower depths affects the balance of energy at each depth through heat capacity terms. This suggests an approach where a differential equation for temperature is written and integrated in s from the initial condition at the trench. Appendix B contains the details and mathematics involved in the development and solution of this equation. Here are mentioned only the effects considered, and one major approximation made.

The sources of thermal energy considered in this calculation are shear-strain heating and the warmth of the deeper parts of the oceanic slab. Energy is assumed to go into seismic radiation, warming of shear zone rocks, conduction into the slab, conduction into the island arc, conduction up- and down-dip within the shear zone and enthalpy of metamorphic reactions. Since some of these terms are temperature-dependent and others are fixed, the steady-state shear zone temperature at each depth can be found by invoking conservation of energy.

In calculating the heat flux out of the top and bottom of the shear zone, it is necessary to deal with conduction in the subducting plate and island arc. The geometry of these is not simple, so either an analytic approximation or a finite-difference numerical computation must be used. In this work the approximation was to make the flow of heat unidirectional, as shown in Fig. 6. Heat travelling upward from the shear zone is presumed to travel vertically, and heat conducted down into the slab is assumed to travel perpendicular to the shear zone surface. These approximations are believed to give fluxes accurate within ±15 per cent, except very near to the point of magma generation and eruption. The problem is that heat conducted laterally from the rising magmas of the volcanic line toward the trench is not considered. Probably a better understanding of the magma-ascent process is needed before this effect can be reasonably estimated.

4.1 TEMPERATURES BELOW TONGA

Many of the parameters involved in the calculation of temperature (such as shear stress) cannot be uniquely specified, but a range of plausible values can be selected. By grouping

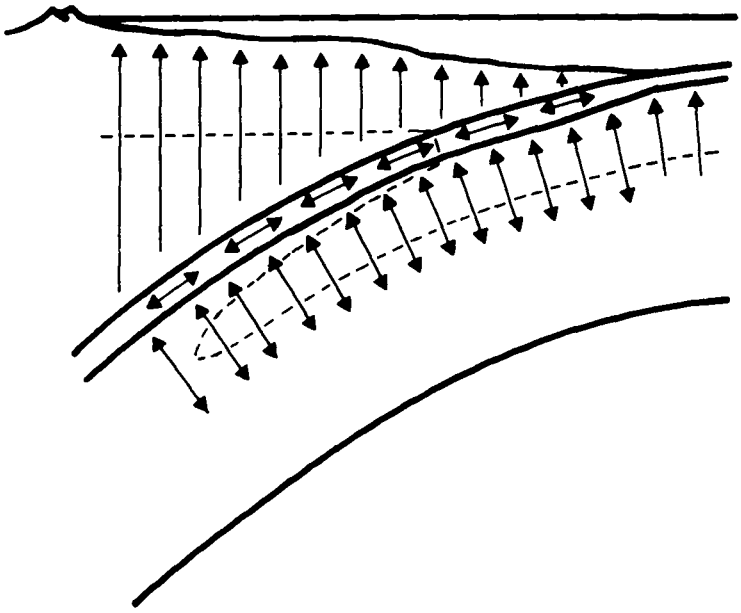

Figure 6. Schematic diagram of a subduction zone showing the directions of heat conduction allowed by the temperature calculation scheme (arrows). The dashed line is a hypothetical isotherm that would be consistent with such behaviour.

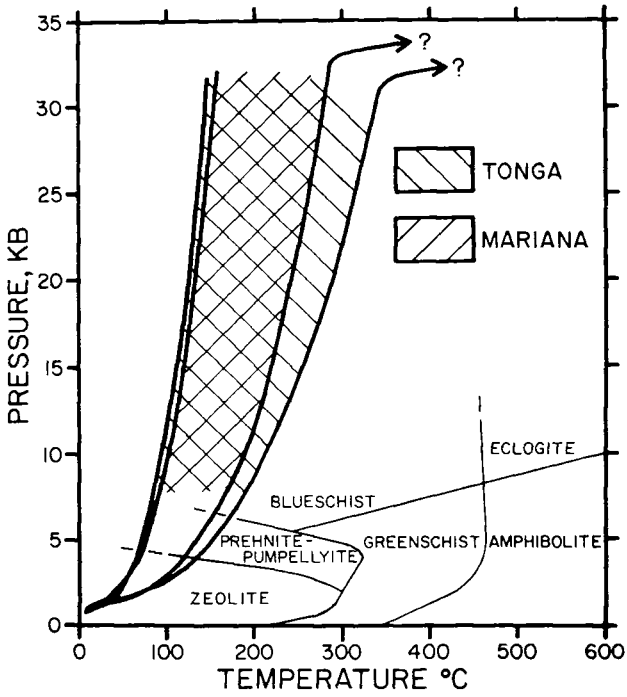

Figure 7. Range of probable temperatures in the Tonga and Mariana shear zones. Also shown are generalized metamorphic facies boundaries of Ernst (1975a).

Table 2. Parameters in shear zone temperature calculations.

Parameter	Symbol	Tonga		Mariana	
		Minimum	Maximum	Minimum	Maximum
		T	T	T	T
Shear zone thickness, m	W	1000	1000	600	600
Subduction velocity, cm/yr	V	8.1	11.1	5	9
Average initial shear zone temperature, °C	T_0	9	9	6	6
Pacific sea-floor heat flux, mW m^{-2}	F_0	41.8	41.8	41.8	41.8
Thermal conductivity, erg/cm s °C	K	3.0×10^5	3.0×10^5	3.0×10^5	3.0×10^5
Heat capacity, erg/g °C	C	1.3×10^7	1.3×10^7	1.3×10^7	1.3×10^7
Average shear stress, bar	$\bar{\tau}_t$	120	320	90	240
Seismic stress drops, bar	$\Delta\tau$	144	0	0	0
Density, g cm^{-3}	ρ	3.3	3.3	3.3	3.3
Mass concentration of metamorphic reactants (I, II), per cent	f	5, 25	0, 0	5, 25	0, 0
Thickness of metamorphic layer (I, II), km	—	4.5, 0.5	—	4.5, 0.3	—
Enthalpy change, low P to high P (I, II), cal/g	ΔH	6.8, −89.4	—	6.8, −89.4	—
Slope of phase boundary (I, II), bar/°C	dp/dt	−60, 215	—	−60, 215	—
Zero-pressure transition temperature, °C	T_0	210, 90	—	210, 90	—

Notes:
I: Prehnite + chlorite + quartz → epidote + tremolite + water.
II: Montmorillinite → pseudo-pyrophillite + water.

together these limiting values, the maximum and minimum temperatures likely to exist in the Tongan shear zone have been determined, and are shown in Fig. 7. Because of the low shear stress, there is little frictional heating, and the temperature reaches only 90–200°C at 30 km depth. By the time the slab passes under the volcanic islands of the Tonga chain, its surface has been heated to only 150–350°C. These temperatures are far lower than any previous estimates of the shear zone geotherm. They are sensitive to such parameters as shear stress, subduction velocity, conductivity and diffusivity; but only slightly affected by such details as shear zone width or metamorphism.

The values of all these parameters are summarized in Table 2 for all the models calculated.

The parameter which is most difficult to select is the thickness of the shear zone. A number is obtained here by assuming that all the sediments on the Pacific floor are subducted into the shear zone. These sediments are more likely to have anomalously high pore pressures developed in them than the crustal basalts. Of course, the thickness estimate could be too large if sediment is scraped off the slab at the trench. This apparently does not happen in Tonga, where Fisher & Engel (1969) report only igneous rocks dredged from the inner slope. Or the thickness could be too low if a lot of sediment is contributed from the island arc side. This is difficult to estimate because the flat trench floor assumed in the model of Helwig & Hall (1974) is not visible on the profiles.

During site surveys for DSDP site 204, two-way seismic travel times of up to 0.50 s were observed in sediments east of the Tonga Trench (Burns *et al.* 1973). This implies about 500 m cover of sediments in this part of the Pacific. However, conservation of volume requires that the shear zone be twice as thick, because its average velocity is only half that of the slab.

The initial slab heat-flow F_0 is not well known in the Tonga area, so a value of 1.0 HFU was selected from the average curve of Sclater, Lawver & Parsons (1975). Thermal conductivity, heat capacity and density values are intended to represent the thermal behaviour of a predominantly olivine mantle at low temperatures (Schatz & Simmons 1972), because most

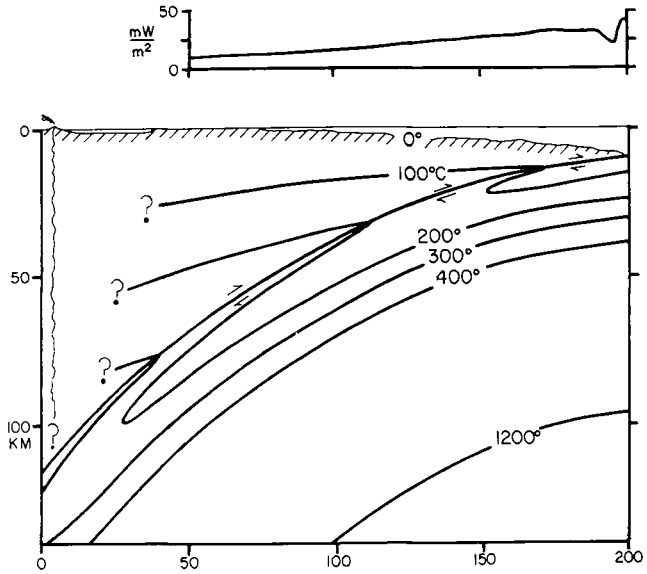

Figure 8. Maximum probable temperatures in the vicinity of the Tonga shear zone, obtained by combining the assumed heat conduction shown in Fig. 6 with the maximum geotherm curve in Fig. 7. Temperature and heat flow are obviously too low near the volcanic line because horizontal heat conduction in the island arc has been excluded.

of the heat is absorbed by the mantle. The model is not sufficiently complex to allow contrasting or temperature-dependent properties.

With these values fixed, both upper- and lower-bound temperatures were calculated for the shear zone by using maximum and minimum values of average stress, plate velocity, dehydration enthalpies and seismic stress drops. The highest temperature is attained if stress drops are negligible ($\bar{\tau}$) and plate velocity (V) are maximized. For Tonga the computed stress maximum is 320 bar, and the maximum likely velocity is 11.1 cm/yr (allowing for 3 cm/yr of back-arc spreading). In this model we also assume negligible dehydration enthalpy. In Fig. 8 temperatures around the shear zone are plotted according to the assumptions of unidirectional conduction illustrated by Fig. 6. These temperatures are clearly too low in the vicinity of the ascending magmas, because lateral conduction of heat from the arc has been excluded. This is also the reason for the low heat flows close to the arc. It should be understood that the calculated temperatures in the deepest part of the shear zone are unrealistically low because of the exclusion of this mechanism.

To compute a lower-bound temperature for Tonga, the lower stress limit is used, the convergence velocity is reduced by assuming only 0.5 cm/yr of back-arc spreading, and an average stress drop of 144 bar is assumed. This last figure is the average of 22 South American shallow subduction-zone stress drops determined by Wyss (1970), when the stress drops are weighted by their corresponding seismic moments. (Note that the value of $\Delta\tau$ in (B3) is twice the value of the 'apparent average stress' as defined by Wyss.)

This model also included two dehydration reactions which might take place in the shear zone. The first is the transformation of prehnite + chlorite + quartz to epidote + tremolite + water, with parameters given by Anderson *et al.* (1976). A second reaction included was the expulsion of inter-layer water from montmorillinite and similar clays, which might plausibly constitute up to 25 per cent of the subducted sediments. The enthalpy change of 89.4 cal/gm was measured by Sudo *et al.* (1967), and the molar volume change was crudely

estimated at 16 $cm^3 mole^{-1}$ from a comparison of montmorillinite and pyrophyllite structures.

However, these phase changes had little effect on the results, since the first has a very small enthalpy and the temperature never became high enough to activate the second! The major difference between this model and the preceding one came from the reduction of stress.

4.2 TEMPERATURES BELOW THE MARIANAS

The probable temperatures calculated for the Mariana Shear Zone fall within the range determined for Tonga, with somewhat lower upper bounds. This is a natural result of the similar geometries, but lower stress and lower (?) subduction velocity of the Mariana plate boundary. Its shear zone geotherm is probably the coldest yet proposed for this planet.

The subduction velocity in the Marianas is very poorly known because the Mariana Trough is spreading at an unknown rate while the Philippine Trench is subducting at an unknown rate. Falling back upon the length of seismic zone method (Isacks *et al.* 1968) it is estimated that the convergence rate is between 5 and 9 cm/yr. Of course, their correlation was established without correcting rates for back-arc spreading.

The thickness of sediments subducted is also less. Seismic reflection at DSDP site #59 showed two-way sediment times of only 0.3 s (Karig 1971c) indicating perhaps 300 m of sediment on the sea-floor. Thus the shear zone thickness was assumed to be 600 m. This and other parameters are summarized in Table 2.

The maximum temperature model for the Marianas had a shear stress of 240 bar with no stress drops, the maximum velocity and no dehydration reactions. Temperatures are slightly cooler than the maximums for Tonga (Fig. 7) at all depths, reaching only 170°C at 30 km depth and 290°C at the bottom.

The minimum temperature model had a shear stress of 90 bar, minimum convergence velocity and the two dehydration reactions outlined in Section 4.1. No stress drops were included because the Mariana is essentially an aseismic arc (McGarr 1977). This model resulted in temperatures close to the Tonga minimums: 93°C at 30 km depth and 157°C at 108 km, directly below the volcanic arc.

5 Metamorphism in subduction zones

Although the temperatures presented here are lower than previous estimates, the predicted metamorphic assemblages to depths of 30 km are hardly different, and agree with many assemblages produced by ancient shear zones. The major change from previous conceptions is in the prediction that most of the hydrous crustal minerals may remain stable throughout their passage through the shear zone, until they are exposed to the asthenosphere near the point of magma genesis.

These calculated temperatures are so low that the dehydration of the minerals serpentine, chlorite, epidote and talc discussed by Anderson *et al.* (1976) apparently does not occur in these two subduction zones. Thus the large amounts of water bound into the oceanic crust by hydrothermal alteration near spreading ridges (Wolery & Sleep 1976) probably remain bound while the upper face of the Pacific slab is in contact with the base of the island arc. The major mineralogical changes to be expected within the calculated regime are analcime + quartz → albite + fluid (Campbell & Fyfe 1955), laumontite or heulandite → lawsonite + quartz + fluid (Nitsch 1968; Liou 1971), calcite → aragonite (Jamieson 1953), and albite → jadeite + quartz (Newton & Smith 1967). None of these will release major amounts of water;

the major sources in these subduction shear zones are probably the dewatering of clays and the breakdown of amphiboles. The first may be important in maintaining high pore pressures in the shear zone, while the second may be important in magma genesis.

While the stress and temperature values for other subduction zones need not be the same as those for Tonga, there is fairly good agreement between predicted and observed metamorphic assemblages. Fig. 7 compares the P–T trajectories with generalized assemblage fields from Ernst (1975a). In either subduction zone, a zeolite facies should form and persist to about 12 km depth, then transform to prehnite-pumpellyite. This in turn would transform to blueschist facies at about 20 km. Actually this same sequence of metamorphic belts, in what are inferred to be exhumed subduction shear zones, has been found in the Franciscan of California, the Sanbagawa zone of Japan, the Kenai–Chugach zone of Alaska, the Torlesse-Haast zone of New Zealand and the Alps (Ernst 1975b). Of course, some of these exposures (Japan, New Zealand, Alps) show higher-temperature facies of greenschist, eclogite or amphibolite succeeding the blueschist in the landward direction. One possible cause of this difference is greater stress and frictional heating in those more continental arcs. It is interesting to speculate that more quantitative petrologic models may eventually make possible the determination of palaeo-stresses.

6 Origin of island arc magmas

The ultimate origin of island-arc lavas has been the subject of speculation and debate for years, chiefly in the form of geochemical arguments that they form from melting of the subducted oceanic crust, or alternatively from the overlying asthenosphere. With these approximate calculated temperatures a thermal constraint can be added to the problem for these two particular island arcs.

Direct melting of the crust from frictional heating is ruled out. According to results of Turcotte & Schubert (1973) this would require an average of 1350 bar of shear, which is excluded unless the error estimates of Section 2 are 10 times too small. The highest temperatures in the crust where friction is the heating mechanism will be about 350°C, as opposed to a probable minimum melting temperature of about 750°C for eclogite at 30 kbar (Lambert & Wylie 1972).

There is still the possibility of an intermediate mechanism in which the crust is melted when it subducts below the island arc lithosphere and suddenly comes into contact with very hot asthenosphere. In the thermal problem where two half-spaces of different temperature are brought into contact, the temperature of the contact surface remains at the average temperature forever. This case is slightly different because one half-space (the slab) has lower temperatures in its interior at the time of contact (Fig. 8). This means that the contact temperature will start at the average value and then decline for at least a million years. Since the asthenosphere temperature must be less than its dry solidus at 1600°C (Kay, Hubbard & Gast 1970), the slab surface temperature below these arcs will not exceed 975°C. For a more plausible asthenosphere temperature of 1350°C, it will not exceed 850°C. But this might be sufficient to melt a water-saturated crustal eclogite.

The difficulty with this contact-melting idea is that Meijer (1976) has shown that the Mariana volcanics have an isotopic composition indicating that they contain no more than 1 per cent of material derived from oceanic sediments. It is difficult to imagine the eclogite crust melting out from underneath the sediments without involving them. It is also difficult to accept that any frictional process could so completely remove the sediments from the rough upper surface of the slab during subduction. A magma-generating mechanism with a source region above the slab is therefore more attractive.

This could be the partial melting of asthenosphere above the slab because water released from its surface diffuses upward and reduces the melting temperature below ambient (Ringwood 1977). At least three sources of water are available, if the speculations of Sections 3 and 5 are correct. There may be sea-water within pore spaces in the subducted sediments. Secondly, the dehydration reactions discussed by Anderson *et al.* (1976) would be suddenly activated by the heat of the asthenosphere into which the slab plunges. Finally, there is the breakdown of amphiboles at about 100 km depth which also releases water (Boettcher 1977). Anderson's (1974) observation that island arc lavas have H_2O/Cl ratios similar to sea-water suggests that the first source is more important than the latter two.

A necessary condition for this mechanism is a continuous supply of fresh hot asthenosphere at a point below the island arc and above the slab, because heat is being lost both upwards and downwards from the asthenospheric wedge. Thus the induced convection above the downgoing slab predicted by McKenzie (1969), Sleep & Toksöz (1971) and Toksöz & Bird (1977) must be operative. Probably the cooling and depleted residue left (after the partial melt has risen toward the surface) becomes attached to the top of the slab and is carried far away from the island arc.

7 Conclusions

Shear stresses and temperatures have been calculated for the interplate shear zones where the subducting Pacific plate is in contact with the Tonga and Mariana island-arc plates. Both of the zones have very low average stresses of a few hundred bars. These stresses were obtained from topographic and gravity data without the need for any knowledge of the internal mechanics of the zones.

Because the Tongan zone is seismic and the Mariana is aseismic at approximately equal stress and velocity, creep of a weak mineral seems to be a poor explanation of these low stresses. More likely, the deformation mechanism is the same frictional type observed in the laboratory at low temperatures. Low shear stress results from low 'effective stress', which is caused by pore pressure within a hundred bars of the least compressive stress. This pore pressure may be created by compaction of sea-floor sediments, and regulated by the pressure-dependence of permeability in the shear zone. While the calculations give no information on the distribution of shear stress with depth, such a mechanism would imply an approximately constant value.

These low stresses imply very low temperatures within the shear zone, up to about 350°C at most. At such temperatures only minor dehydration reactions will occur and there is no question of melting. The predicted metamorphic sequence of zeolite to prehnite-pumpellyite to blueschist facies is in good agreement with exposures from older exhumed shear zones, although some also contain higher-temperature facies suggesting more frictional heating.

This low-temperature environment suddenly changes when the subducting slab comes in contact with hot asthenosphere below the volcanic line. This hot asthenosphere is continually renewed by convection induced by the downgoing slab. The sudden heating it imparts to the slab might melt it, and would certainly trigger a set of dehydration reactions releasing water into the overlying mantle. The effect of this water would be partially to melt that hot mantle, producing the magmas which appear (after some differentiation) in the island arc.

Acknowledgments

This work could not have been completed without the helpful suggestions and information provided by many people. D. Karig, J. Hawkins and D. Hayes helped in locating the necessary basic data. G. Schubert, D. Yuen and L. Fleitout criticized and helped to improve the

method used to calculate temperatures. G. Ernst and A. Boettcher suggested some implications of the conclusions for subduction zone metamorphism and magma generation. The calculations were supported by the Campus Computing Network of the University of California, Los Angeles.

References

Anderson, A. T., 1974. Chlorine, sulfur, and water in magmas and oceans, *Geol. Soc. Am. Bull.*, **85**, 1485–1492.

Anderson, R. N., 1975. Heat flow in the Mariana marginal basin, *J. geophys. Res.*, **80**, 4043–4048.

Anderson, R., Uyeda, S. & Miyashiro, A., 1976. Geophysical and geochemical constraints at converging plate boundaries – I. Dehydration in the downgoing slab, *Geophys. J. R. astr. Soc.*, **44**, 333–357.

Blackwell, D. D. & Ziagos, J., 1977. Heat flow and the thermal effects of subduction in southern Mexico, *EOS Trans. AGU*, **58**, 1233.

Boettcher, A., 1977. The role of amphiboles and water in circum-Pacific volcanism, in *High pressure research: applications in geophysics*, 664 pages, eds Manghnani, M. & Akimoto, S., Academic Press, London.

Bulirsch, R. & Stoer, J., 1966. Numerical treatment of ordinary differential equations by extrapolation methods, *Numer. Math.*, **8**, 1.

Burns, R., Andrews, J. *et al.*, 1973. *Init. rep. Deep Sea Drilling Proj.*, **21**, 33–56.

Campbell, A. & Fyfe, W., 1955. Analcime-albite equilibria, *Am. J. Sci.*, **263**, 807–816.

Carslaw, H. & Jaeger, J., 1959. *Conduction of heat in solids*, p. 63, Clarendon Press, Oxford.

Ernst, W. G., 1975a. Summary, in *Metamorphism and plate tectonic regimes*, pp. 423–426, ed. Ernst, W. G., Halsted Press.

Ernst, W. G., 1975b. Systematics of large-scale tectonics and age progressions in Alpine and circum-Pacific blueschist belts, *Tectonophys.*, **26**, 229–246.

Ewart, A. & Bryan, W. B., 1973. The petrology and geochemistry of the Tongan Islands, in *The Western Pacific; island arcs, marginal seas, geochemistry*, pp. 503–522, University of Western Australia Press, Nedlands.

Fisher, R. L. & Engel, C. G., 1969. Ultramafic and basaltic rocks dredged from the nearshore flank of the Tonga Trench, *Geol. Soc. Am. Bull.*, **80**, 1373–1378.

Hasebe, K., Fujii, N. & Uyeda, S., 1970. Thermal processes under island arcs, *Tectonophys.*, **10**, 335–355.

Hayes, D. E., Talwani, M., Houtz, R. & Pitman, W. C. III, 1972. Bathymetric, geomagnetic, and gravity profiles, in *Preliminary report of volume 22, U.S.N.S. Eltanin cruises 28–32, March 1967–March 1968*, 232 pages, Lamont–Doherty Geological Observatory, Palisades, New York.

Heard, H. C., 1972. Steady-state flow in polycrystalline halite at pressure of 2 kilobars, *Am. geophys. Un. Monogr.*, **16**, 191–209.

Heezen, B. C., MacGregor, I. D., Foreman, H. P., Forristal, G., Hekel, H., Hesse, R., Hoskins, R. H., Jones, E. J. W., Kaneps, A., Krasheninnikov, V. A., Okada, H. & Ruef, M. H., 1973. Diachronous deposits: a kinematic interpretation of post Jurassic sedimentary sequence on the Pacific plate, *Nature*, **242**, 25–32.

Helwig, J. & Hall, G. A., 1974. Steady-state trenches?, *Geology*, **2**, 309–316.

Isacks, B., Oliver, J. & Sykes, L. R., 1968. Seismology and the new global tectonics, *J. geophys. Res.*, **73**, 5855–5899.

Isacks, B., Sykes, L. R. & Oliver, J., 1969. Focal mechanisms of deep and shallow earthquakes in the Tonga–Kermadec region and the tectonics of island arcs, *Geol. Soc. Am. Bull.*, **80**, 1443–1470.

Isacks, B. L. & Barazangi, M., 1977. Geometry of Benioff zones: lateral segmentation and downwards bending of the subducted lithosphere, in *Island arcs, deep sea trenches, and back arc basins*, pp. 99–114, eds Talwani, M. & Pitman, W. C. III, AGU, Washington.

Jamieson, J. C., 1953. Phase equilibria in the system calcite-aragonite, *J. Chem. Phys.*, **21**, 1389–1390.

Karig, D. E., 1970. Ridges and basins of the Tonga–Kermadec island arc system, *J. geophys. Res.*, **75**, 239–254.

Karig, D. E., 1971a. Origin and development of marginal basins in the western Pacific, *J. geophys. Res.*, **76**, 2542–2561.

Karig, D. E., 1971b. Structural history of the Mariana island arc system, *Geol. Soc. Am. Bull.*, **82**, 323–334.

Karig, D. E., 1971c. Site surveys in the Mariana area, Scan IV, *Init. rep. Deep Sea Drilling Proj.*, **6**, 681–689.

Karig, D. E., 1975. Basin genesis in the Philippine sea, *Init. rep. Deep Sea Drilling Proj.*, **31**, 857–880.
Karig, D. E., Caldwell, J. G. & Parmentier, E. M., 1976. Effects of accretion on the geometry of the descending lithosphere, *J. geophys. Res.*, **81**, 6281–6291.
Katsumata, M. & Sykes, L. R., 1969. Seismicity and tectonics of the western Pacific: Izu-Mariana, Caroline, and Ryukyu–Taiwan regions, *J. geophys. Res.*, **74**, 5923–5948.
Kay, R., Hubbard, N. J. & Gast, P. W., 1970. Chemical characteristics and origin of oceanic ridge volcanic rocks, *J. geophys. Res.*, **75**, 1585–1613.
Kuster, G. T. & Toksöz, M. N., 1974. Velocity and attenuation of seismic waves in two-phase media: Part II. Experimental results, *Geophysics*, **39**, 607–618.
Lachenbruch, A. H., 1976. Dynamics of a passive spreading center, *J. geophys. Res.*, **81**, 1883–1902.
Lambert, I. B. & Wyllie, P. J., 1972. Melting of gabbro (quartz eclogite) with excess water to 35 kilobars, with geologic applications, *J. Geol.*, **80**, 693–708.
Le Pichon, X., Franchetau, J. & Bonnin, J., 1976. *Plate tectonics*, pp 48–53, Elsevier, Amsterdam.
Liou, J. G., 1971. Synthesis and stability relations of prehnite, $Ca_2Al_2Si_3O_{10}(OH)_2$, *Am. Miner.*, **56**, 507–531.
McGarr, A., 1977. Seismic moments of earthquakes beneath island arcs, phase changes, and subduction velocities, *J. geophys. Res.*, **82**, 256–264.
McKenzie, D. P., 1969. Speculations on the consequences and causes of plate motions, *Geophys. J. R. astr. Soc.*, **18**, 1–32.
Meijer, A., 1976. Pb and Sr isotopic data bearing on the origin of volcanic rocks from the Mariana island-arc system, *Geol. Soc. Am. Bull.*, **87**, 1358–1369.
Morgan, W. J., 1972. Plate motions and deep mantle convection, ed. Shagam, R., in Hess Volume, *Geol. Soc. Am. Mem.*, **132**, 7–22.
Newton, R. C. & Smith, J. V., 1967. Investigations concerning the breakdown of albite at depth in the Earth, *J. Geol.*, **75**, 268–286.
Nitsch, K. H., 1968. Die Stabilitat Von Lawsonit, *Naturwiss.*, **55**, 388.
Ringwood, A. E., 1977. Petrogenesis in island arc systems, in *Island arcs, deep sea trenches and back-arc basins*, pp. 311–324, eds Talwani, M. & Pitman, W. C. III, Am. Geophys. Un., Washington.
Schatz, J. F. & Simmons, G., 1972. Thermal conductivity of earth materials at high temperatures, *J. geophys. Res.*, **77**, 6966–6983.
Schmid, S. M., 1976. Rheological evidence for changes in the deformation mechanism of Solnhofen limestone towards low stresses, *Tectonophys.*, **31**, T21–T28.
Sclater, J. G., Anderson, R. N. & Bell, M. L., 1971. Elevation of ridges and evolution of the central eastern Pacific, *J. geophys. Res.*, **76**, 7888–7915.
Sclater, J. G., Lawver, L. A. & Parsons, B., 1975. Comparison of long-wavelength residual elevation and free air gravity anomalies in the north Atlantic and possible implications for the thickness of the lithospheric plate, *J. geophys. Res.*, **80**, 1031–1052.
Sleep, N. H., 1973. Deep structure and geophysical processes beneath island arcs, *PhD thesis*, Massachusetts Institute of Technology, Cambridge.
Sleep, N. H., 1975. Stress and flow beneath island arcs, *Geophys. J. R. astr. Soc.*, **42**, 827–857.
Sleep, N. H. & Toksöz, M. N., 1971. Evolution of marginal basins, *Nature*, **233**, 548–550.
Sudo, T., Shimoda, S., Nishigaki, S. & Aoki, M., 1967. Energy changes in dehydration processes of clay minerals, *Clay Miner.*, **7**, 33–42.
Toksöz, M. N. & Bird, P., 1977. Formation and evolution of marginal basins and continental plateaus, in *Island arcs, deep sea trenches, and back arc basins*, pp. 379–394, eds Talwani, M. & Pitman, W. C. III, Am. Geophys. Un., Washington.
Turcotte, D. L. & Schubert, G., 1973. Frictional heating of the descending lithosphere, *J. geophys. Res.*, **78**, 5876–5886.
Watts, A. B., 1976. Gravity field of the northwest Pacific Ocean basin and its margin: Philippine Sea, *Geol. Soc. Am. Map-Chart Series* MC-12.
Weissel, J. K., 1977. Evolution of the Lau Basin by the growth of small plates, in *Island arcs, deep sea trenches, and back arc basins*, pp. 429–436, eds Talwani, M. & Pitman, W. C. III, Am. Geophys. Un., Washington.
Wolery, T. J. & Sleep, N. H., 1976. Hydrothermal circulation and geochemical flux at mid-ocean ridges, *J. Geol.*, **84**, 249–275.
Wyss, M., 1970. Stress estimates for South American shallow and deep earthquakes, *J. geophys. Res.*, **75**, 1529–1544.
Yuen, D. A., Fleitout, L., Schubert, G. & Froidevaux, C., 1978. Shear deformation zones along major transform faults and subducting slabs, *Geophys. J. R. astr. Soc.*, **54**, 93–119.

Appendix A: calculation of shear zone stress

Because the island arc plates are accelerating at completely negligible rates, the forces exerted upon them must be in balance. In this paper we consider only forces acting in the horizontal direction (x) perpendicular to the trend of the island arc. These forces all arise from boundary stresses (σ_{ij}) acting in the (x, z) plane, where z is the vertical dimension. The out of plane stress component σ_{xy} is assumed to be zero, so we seek a balance between the boundary integrals of the components σ_{xx} and σ_{xz}.

Using the points identified in Fig. 1, we require:

$$\int_a^b \sigma_{xx}\,dz + \int_b^c \sigma_{xz}\,dx = \int_c^d [\sigma_{xx}\cos(\boldsymbol{\eta}, \mathbf{x}) - \sigma_{xz}\cos(\boldsymbol{\eta}, \mathbf{z})]\,ds + \int_d^e \sigma_{xx}\,dz \tag{A1}$$

where $\boldsymbol{\eta}$ is the normal vector of the subduction shear zone surface. Next we invoke the four assumptions introduced in Section 2. Because of assumption (1) the second term of the first equation drops out; there is no shear traction on the base of the island arc. Using (1) and (2) the first term becomes:

$$\int_a^b \sigma_{xx}\,dz = \int_0^h \rho_w g z\,dz + \int_h^b (\rho_a g(z-h) + \rho_w g h)\,dz = g\left[\rho_w h\left(b - \frac{h}{2}\right) + \tfrac{1}{2}\rho_a (b-h)^2\right] \tag{A2}$$

where h is the depth of the ocean over the ridge, g is the acceleration of gravity and ρ_w is the density of sea-water. This term must be balanced by forces transmitted through the shear zone.

A Mohr's circle (Fig. 9) will illustrate the calculation of stress components in this zone. If θ is the dip angle of the fault at a point where the maximum shear stress is τ, then from the diagram:

$$\sigma_{xx} = \sigma_{zz} + 2\tau\sin(2\theta) \tag{A3}$$

$$\sigma_{xz} = -\tau\cos(2\theta). \tag{A4}$$

Using (A3) and (A4), the shear zone term of (A1) becomes:

$$\int_c^d [\sigma_{xx}\cos(\boldsymbol{\eta}, \mathbf{x}) - \sigma_{xz}\cos(\boldsymbol{\eta}, \mathbf{z})]\,ds = \int_c^d \sigma_{zz}\sin(\theta)\,ds + \int_c^d \tau\,[2\sin(2\theta)\sin(\theta) + \cos(2\theta)\cos(\theta)]\,ds. \tag{A5}$$

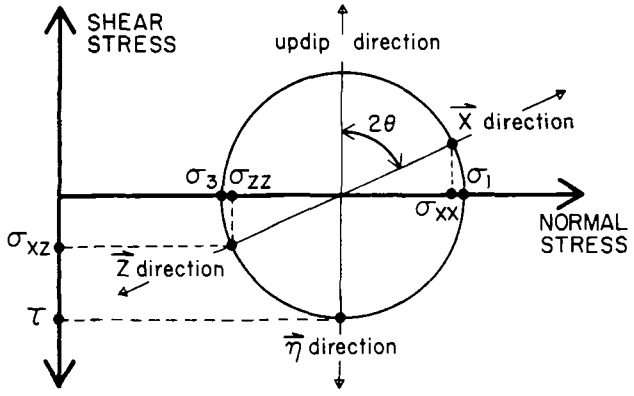

Figure 9. A Mohr's circle representation of stress at one point in the shear zone. Directions from the centre of the circle correspond to orientations of vectors, including the normal to the shear zone $\boldsymbol{\eta}$. Complete explanation in the text.

Combining (A1) through (A5) we obtain an expression for a weighted integral of the shear stress τ on the shear zone:

$$\int_c^d \tau\,[2\sin(2\theta)\sin(\theta)+\cos(2\theta)\cos(\theta)]\,ds = g\left[\rho_w h\left(b-\frac{h}{2}\right)+\frac{\rho_a}{2}(b-h)^2\right]-\int_c^d \sigma_{zz}\,dz - \tfrac{1}{2}g\rho_w d^2. \tag{A6}$$

Now, for the range of dips encountered (4–50°) the weighting factor applied to τ inside the integral varies between 1.007 and 2.0. This means that a unit shear stress in the middle of the subduction zone has almost twice the effect on horizontal force of a unit shear near the top or bottom. With this in mind, the 'average shear stress' $\bar{\tau}$ which is defined by

$$\bar{\tau} \equiv \frac{\displaystyle\int_c^d \tau\,[2\sin(2\theta)\sin(\theta)+\cos(2\theta)\cos(\theta)]\,ds}{\displaystyle\int_c^d [2\sin(2\theta)\sin(\theta)+\cos(2\theta)\cos(\theta)]\,ds} \tag{A7}$$

must be considered a weighted average.

In order to evaluate (A6) the vertical stress σ_{zz} must be known. It is assumed (4) that this stress is equal to the weight of overburden, but gravity data are needed to estimate this accurately. In the simple reference structure of Fig. 2, this vertical stress is easily calculated as

$$\sigma_{zz}^* = \rho_a g(z^* - f) + \rho_w g f \tag{A8}$$

where z^* is the depth to the top of the slab. Thus any difference between actual gravity and model gravity ($\Delta g - \Delta g^*$) must be the smoothed result of differences in overburden weight between the actual structure and the model. Because gravity is a conservative field, its integral gives the integral of the anomalous mass per unit area:

$$\frac{1}{g}\int(\sigma_{zz}-\sigma_{zz}^*)\,dx = \frac{1}{2\pi G}\int(\Delta g-\Delta g^*)\,dx \tag{A9}$$

where G is the universal gravitational constant and the stresses are evaluated at the top of the slab. Unfortunately, the term which is required is

$$\int_c^d \sigma_{zz}\,dz = \int_c^d \sigma_{zz}\tan(\theta)\,dx = \int_c^d [\rho_a g(z^*-f)+\rho_w g f]\tan(\theta)\,dx + \int_c^d (\sigma_{zz}-\sigma_{zz}^*)\tan(\theta)\,dx. \tag{A10}$$

So it is necessary to approximate the last term of (A10) by using (A9):

$$\int_c^d (\sigma_{zz}-\sigma_{zz}^*)\tan(\theta)\,dx \simeq \frac{g}{2\pi G}\int_c^d (\Delta g-\Delta g^*)\tan(\theta)\,dx. \tag{A11}$$

This is a good approximation because the smoothing effect of gravity takes place with no phase shift over a wavelength comparable to the depth of the anomalous masses. These are mainly the topography and sediments which are 0–10 km below the observer. Within such a horizontal range the variation of the weighting function $\tan(\theta)$ is almost linear. In any case, errors introduced by approximation (A11) affect only the second term on the right hand side of (A10), which is a very small fraction of the total horizontal force term.

We have finally obtained the weighted average shear stress in the upper subduction zone in terms of available observables (ocean depths and gravity and depth of the slab), a density

which is well known (ρ_w), and another which need only be approximately correct (ρ_a):

$$\bar{\tau} \simeq \left\{ g\left[\rho_w h\left(b - \frac{h}{2}\right) + \frac{\rho_a}{2}(b-h)^2\right] - \tfrac{1}{2} g \rho_w d^2 - \int_c^d \left[\rho_a g(z^* - f) + \rho_w g f\right] dz \right.$$

$$\left. - \frac{g}{2\pi G}\int_c^d (\Delta g - \Delta g^*) \tan(\theta)\, dx \right\} \cdot \left\{ \int_c^d \left[2\sin(2\theta)\sin(\theta) + \cos(2\theta)\cos(\theta)\right] ds \right\}^{-1}. \tag{A12}$$

Appendix B: calculation of shear zone temperatures

We solve the heat equation under the assumption of steady-state subduction conditions. The calculation is reduced to a single independent variable, the distance into the shear zone in the downdip direction (s), by neglecting variation of temperature through the thickness of the shear zone and working with a one-dimensional dependent variable $T(s)$. Then conservation of energy requires

$$\left[\frac{V\rho C}{2}\right]\frac{dT}{ds} = K\frac{d^2T}{ds^2} + Q_{\text{fric}} + Q_{\text{react}} + \frac{1}{W}(F_{\text{up}} + F_{\text{down}}). \tag{B1}$$

In this equation V is subducting plate velocity, ρ is density, C is specific heat, K is thermal conductivity and W is the width of the shear zone. Q_{fric} and Q_{react} are the volumetric heat productions from shear-strain heating and metamorphic reactions respectively. F_{up} and F_{down} are heat fluxes through the top and bottom surfaces of the shear zone, with inward flux considered positive.

The frictional heating term is simply:

$$Q_{\text{fric}} = \tau \frac{V}{W} \tag{B2}$$

regardless of the mechanism of creep. However, if there is seismic deformation, energy is released in seismic waves and Q_{fric} is less. Consider the simple model of an earthquake

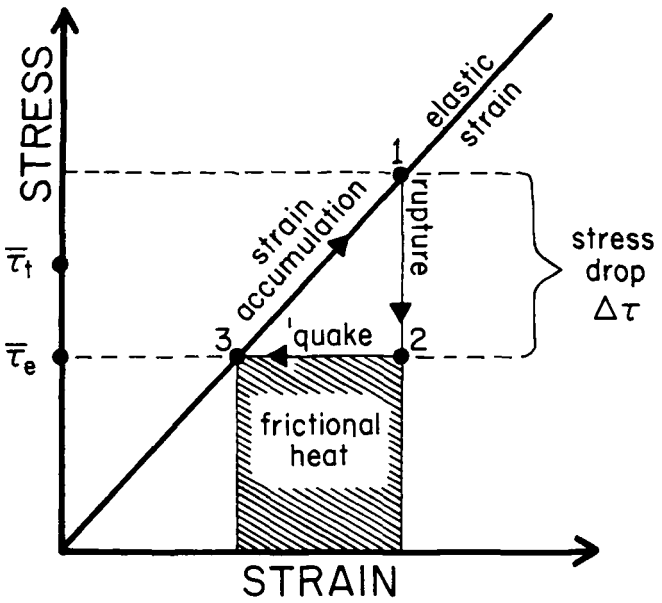

Figure 10. A simple model for stress and strain accumulation and release by an earthquake. If an instantaneous stress drop $\Delta\tau$ is followed by unstraining, the shaded area represents work dissipated as heat, and the remainder is seismic energy radiated away. Average stresses defined in the text.

illustrated in Fig. 10. If an earthquake can be considered as an instantaneous stress drop followed by frictional sliding, then the stress appropriate for (B2) is the strain-averaged stress $\bar{\tau}_e$. However, most of the time in the earthquake cycle is spent in strain accumulation, and the stress which is important in the force balance of the island arc is the time-averaged stress $\bar{\tau}_t$. This is larger:

$$\bar{\tau}_t = \bar{\tau}_e + \tfrac{1}{2}\Delta\tau. \tag{B3}$$

Thus (B2) should be rewritten in the case of seismic slip to read

$$Q_{\text{fric}} = (\tau_t - \tfrac{1}{2}\Delta\tau)\frac{V}{W} \tag{B4}$$

so that the stresses determined in Section 2 can be employed. τ_t could be modelled as dependent upon T, V, W, θ, s or several other variables, but in this paper is held constant.

The metamorphic reaction term is zero except when passing through a transition, which is assumed to be spread over a finite pressure interval for convenience. Assume that a reaction begins at pressure P_0 (at zero temperature) and ends at $(P_0 + \Delta P)$. Also assume that the metamorphic facies boundaries have constant slope (dP/dT). If ΔH is the specific enthalpy change on transformation to the high-pressure phase, the heat production term is:

$$Q_{\text{react}} = -\Delta H \rho f \left[\frac{1}{\Delta P}\frac{dP}{dS} - \frac{(dP/dT)}{\Delta P}\frac{dT}{ds}\right] \tag{B5}$$

where f is the fractional concentration of reactants. There may be a sum of such terms if several different reactions are underway simultaneously. The main equation (B1) is still linear, however, because all of the coefficients of (dT/ds) in (B5) are constants.

The calculation of fluxes out of the shear zone employs the one-dimensional approximation explained in Section 4 and Fig. 6.

In a steady-state model with negligible radioactive heat production, all the heat flux at the surface must come from the shear zone, and there will be a linear temperature variation in any vertical column. Then F_{up} is just the flux required to maintain this gradient, with a correction for the dip angle (θ) of the subduction zone:

$$F_{\text{up}} = K(T_w - T)\cos(\theta)/h(s) \tag{B6}$$

where T_w is the temperature of bottom sea-water and $h(s)$ is the depth of the shear zone below the sea-floor.

With the one-dimensional approximation above, the conducting slab can be modelled as a semi-infinite half-space with an initially linear temperature gradient, that then has a specified continuous thermal history imposed upon its surface. The initial gradient is associated with the steady-state pre-subduction heat flow F_0, and the subsequent surface temperatures are the values of $T(s)$ for smaller s. The problem is to find the surface flux (F_{down}) at the end of that history.

A generalized integral solution to this problem has not been found, and so it is necessary at this point to introduce numerical methods. We switch from spatial to time coordinates by following a portion of the slab as it subducts and using the transformation:

$$t = s/V. \tag{B7}$$

If we have previously determined the shear zone temperature $T(s)$ at equally spaced points shallower than the one in question, this transformation converts them to $T(t)$ in the slab frame, with time interval Δt. To interpolate between these points, we use polynomials in time for which the solution in a half-space is known. To insure continuity of F_{down}, there

must be no discontinuity in (dT/dt) at these points. Thus we use a staggered sum of weighted $(t^{3/2})$ functions to represent the past slab surface temperature.

That is, the N known temperatures T_i at times $t = 1\Delta t, 2\Delta t \ldots N\Delta t$ are used to determine the N coefficients k_i of the approximation:

$$T(t) = \sum_{i=1}^{(\leqslant t/\Delta t)} k_i [t - (i-1)\,\Delta t]^{3/2}. \tag{B8}$$

This approximation has a continuous derivative, implying a piecewise-linear and continuous $F_{\text{down}}(t)$. Its solution in terms of coefficients k_i is obtained from the relations:

$$k_1 = T_1 \Delta t^{-3/2}; \quad k_{i+1} = \left[T_{i+1} - \sum_{j=1}^{i} k_i [(i-j+2)\,\Delta t]^{3/2}\right] \Delta t^{-3/2}. \tag{B9}$$

The value of this series is that it gives an analytic solution (Carslaw & Jaeger 1959) for the temperature inside the slab which, when differentiated, gives the surface flux:

$$\begin{aligned}(F_{\text{down}})_i &= F_0 - K \sum_{j=1}^{i} \left.\frac{d}{dz}\right|_{z=0} \left\{k_j \Gamma(5/2)\,[4(i-j)\,\Delta t]^{3/2}\, i^3 \operatorname{erfc}\left[\frac{z/2}{\sqrt{\kappa (i-j)\,\Delta t}}\right]\right\} \\ &= F_0 - (1.329) K \frac{\Delta t}{\sqrt{\kappa}} \sum_{j=1}^{i} (1 + i - j)\, k_j.\end{aligned} \tag{B10}$$

In this equation κ is the thermal diffusivity. This completes the identification of terms in equation (B1).

To solve equation (B1) for temperature, we note that the second term is small compared with others. When it is dropped, and the resulting first-order linear equation is solved, the results give an approximation at each solution point $(s_i = i\Delta s)$:

$$K \frac{d^2 T}{ds^2} \approx \frac{K}{(\Delta s)^2} (T_{i+1} - 2T_i + T_{i-1}). \tag{B11}$$

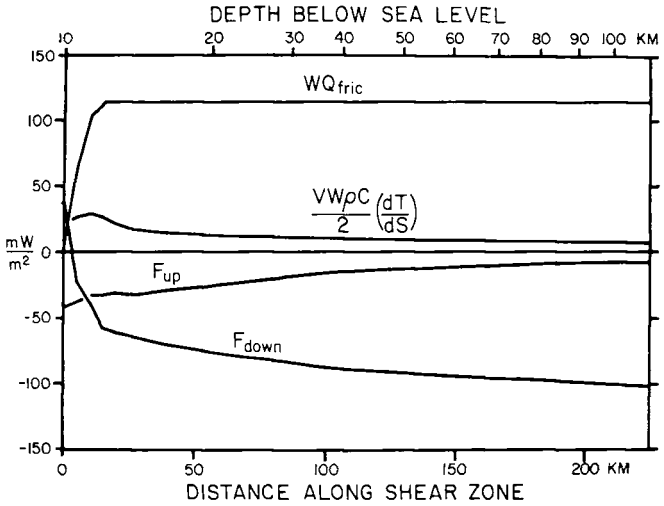

Figure 11. Variation of the terms in the heat balance for the maximum temperature Tonga model as a function of distance into the shear zone. Down-dip conduction effect is too small to plot.

This approximation was used as a correction in the second iteration, and by the third iteration a stable solution was found.

Within each of the three iterations, the solution to the first-order equation was found by one of two methods. Preferably the equation is numerically integrated by the step-size extrapolation method of Bulirsch & Stoer (1966) with a starting step-size of $\Delta s = 5$ km. In this case the numerical error can be controlled to $\pm 2°$C. However, the volatility of the equation for (dT/ds) increases rapidly as the shear zone is made thinner or as the plate velocity is reduced. For products (VW) of less than 0.019 cm^2 s^{-1} this extrapolation method becomes unstable and fails. In this case the equation was solved by collocation at discrete points 5 km apart, with the derivative approximation:

$$\left(\frac{dT}{ds}\right)_i \approx \frac{1}{2\Delta s}(T_{i+1} - T_{i-1}). \tag{B12}$$

An error limit for collocation cannot be set, but comparison of the two methods in the domain where they both work suggests that collocation results are good to $\pm 10°$C.

Tonga models were computed by the step-size extrapolation method, but Mariana models had to be done by collocation because of the thinner shear zone and lower plate velocity.

Fig. 11 gives more details concerning one of the solutions by plotting each term of equation (B1) separately as a function of s. The term $K(d^2T/ds^2)$ is too small to plot.